Measurement of Dissolved Oxygen and Its Diffusivity in Aerobic Granules Using a Lithographically-Fabricated Microelectrode Array

ARTICLE *in* ENVIRONMENTAL SCIENCE AND TECHNOLOGY · JANUARY 2009

Impact Factor: 5.33 · DOI: 10.1021/es802662e

8 AUTHORS, INCLUDING:

Shaoyang Liu
Troy University
26 PUBLICATIONS **318** CITATIONS
SEE PROFILE

Han-Qing Yu
University of Science and Technology of C…
508 PUBLICATIONS **11,050** CITATIONS
SEE PROFILE

Gang Liu
University of Science and Technology of C…
84 PUBLICATIONS **1,014** CITATIONS
SEE PROFILE

Environ. Sci. Technol. **2009,** *43,* 1160–1165

Measurement of Dissolved Oxygen and Its Diffusivity in Aerobic Granules Using a Lithographically-Fabricated Microelectrode Array

SHAO-YANG LIU,[†] YOU-PENG CHEN,[†] FANG FANG,[†] JUAN XU,[†] GUO-PING SHENG,[†] HAN-QING YU,*[,†] GANG LIU,[‡] AND YANG-CHAO TIAN[‡]

Department of Chemistry, University of Science and Technology of China, Hefei, 230026, China, and National Synchrotron Radiation Laboratory, University of Science and Technology of China, Hefei, 230026, China

Received September 18, 2008. Revised manuscript received December 17, 2008. Accepted December 18, 2008.

A novel gold microelectrode array (MEA) was manufactured with microfabrication techniques and applied on the measurement of dissolved oxygen profile in an aerobic granule. The MEA contained five gold microelectrodes, which had a good linear response to dissolved oxygen and typically had a lifetime of more than 10 days. Dissolved oxygen microprofiles near the surface of an aerobic granule were monitored with this MEA. Based on the measurements, an oxygen effective diffusivity in the upper 100 μm layer of the aerobic granule was estimated to be 1.19×10^{-9} m^2/s. The experimental results demonstrate that the MEA was able to measure the DO levels in aerobic granules accurately and precisely and that the MEA could be used to determine constituents, profiles, and functions in situ in small spaces. Moreover, since the device shape and microelectrode arrangement were all defined by photolithography, the proposed fabrication procedure was flexible and appropriate for fabrication of various types of MEAs.

Introduction

Microelectrode array (MEA) is one of the most attractive detection tools in environmental (*1*−*3*), biological (*4*), chemical (*5, 6*), and medical (*7, 8*) areas. MEAs keep all the advantages of microelectrodes, e.g., rapid response, high signal-to-noise ratio, low requirement of electrolyte concentration, and ability for in situ analysis. They also have extra merits associated with the deliberated designs and/or operational methods. Microelectrodes on an MEA could be used to restrain noise and drift of signal (*1, 9*), or to amplify amperometric responses (*10, 11*). In addition, they could also be used separately for simultaneous measurement of different samples (*12, 13*) or parameters (*14*).

Because of different requirements, numerous types of MEAs with special shapes and electrode arrangements are desired. Thus, a flexible MEA fabrication procedure is highly preferred. Since conventional pulling-micropipette procedures are not appropriate to manufacture multisensors, microfabrication techniques are introduced for the development of MEAs (*15, 16*). However, the shape of silicon/glass devices is not readily controlled (*9, 17, 18*). Recently, a glass-based MEA containing four needle-type microelectrodes was fabricated with a dynamic etching technique. However, the etching procedure is complicated, and the interval between the two neighboring microelectrodes was relatively large (0.9 mm) (*19, 20*). In our previous work, an easy shape-controlling procedure for microelectrode fabrication was proposed, following which the microelectrode shape was facilely defined by photolithograph on a negative photoresistant (*21*). With this method, we fabricated a series of needle-type microelectrodes which contained two working electrodes and could fulfill two-channel measurement (*21, 22*). However, similar to conventional pulling-micropipette ones, the working electrodes have to locate at the end of the needle. Thus, our previous design and fabrication procedure only provide the freedom of device shape control, but not microelectrode arrangement, which just meet one aspect of the requirements for multichannel analysis at multiposition.

In the present work, a developed design was proposed for convenient electrode arrangement, and a fabrication procedure was established to fulfill it without sacrificing the facility of device shape control. Following this procedure, a novel needle-type gold MEA was fabricated for multianalysis of environmental samples. This newly fabricated MEA contained five working electrodes located along the axis on the needle surface. Thus, it had a potential of five-channel determination at different positions. Gold was selected as the electrode material because of it versatility. It could be used for dissolved oxygen (DO) measurement (*23, 24*) and had great functionalizing potentials (*25, 26*).

Aerobic-granule-based process is a promising technique for wastewater treatment (*27*−*29*). Previous works indicated that the granules were delaminated and that its outer layer was the most active part (*21, 30, 31*). In this work, a set of DO concentrations was measured with the fabricated MEA by only inserting into an aerobic granule once. Then, a mathematical model, taking oxygen diffusion and consuming into account, was employed to estimate the oxygen effective diffusivity (D_{eff}) and the DO consumption kinetic parameters in the upper 100 μm layer of the granule based on the measured DO levels. Since DO is a critical factor in a variety of biomedical and environmental processes, measured DO and related parameters, e.g., the oxygen diffusivity and the DO transport flux, are helpful to achieve a better understanding of aerobic granules.

Experimental Section

Chemicals. Ethanol, isopropanol, sodium hydroxide, potassium ferricyanide, potassium ferrocyanide, and potassium chloride, all purchased from Shanghai Chemical Reagent Company, were of analytical grade and used as received. Deionized water was used throughout the experiments.

Microfabrication of MEA. Each glass plate substrate was patterned to contain six MEAs for mass production. The fabrication procedures are described in Figure 1.

Supporting SU-8 Layer Fabrication. The glass plate (65 × 65 × 2 mm) was washed with detergent and rinsed with water and acetone, and dried in an oven at 110 °C for 30 min. The glass plate was spin-coated with a thin layer of OmniCoat (MicroChem, U.S.) at 2000 rpm for 30 s as adhesive and baked at 200 °C for 2 min on a hot plate. Then, a 90-μm-thick SU-8 (SU-8 2100, MicroChem, U.S.) layer was applied as the supporting layer of the MEAs. The SU8 layer was soft-baked

* Corresponding author fax: +86 551 3601592; e-mail: hqyu@ustc.edu.cn.
[†] Department of Chemistry.
[‡] National Synchrotron Radiation Laboratory.

10.1021/es802662e CCC: $40.75
Published on Web 01/23/2009

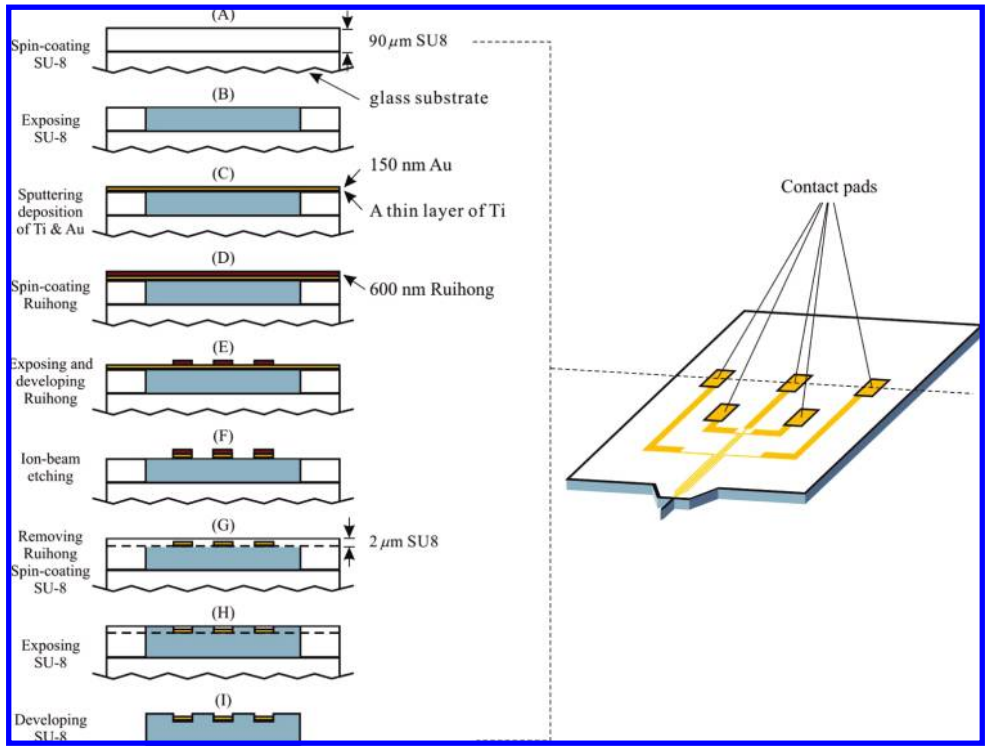

FIGURE 1. Schematic diagram of the fabrication procedures for the innovative MEA (For clarity, only one MEA is shown).

at 65 °C for 10 min and 95 °C for 60 min on a level hot plate (Figure 1, A), and patterned using a photomask of the MEA shape (i-line, 200 mJ/cm^2). An oven was used for post exposure bake (PEB) (65 °C for 5 min; rise to 95 °C with a ramp of 2 °C/min; 95 °C for 30 min) (Figure 1B). After baking SU-8, the substrate was allowed to cool down to ambient temperatures on the hot plate or in the oven to release stress.

Metal Track Formation. Sputtering deposition was employed for metal track formation on the SU-8 layer. A 150-nm-thick gold layer was deposited as the conductive material of the microelectrode after the deposition of a thin titanium layer, which was used to improve the adhesion between the gold and the substrate (Figure 1C). Subsequently, a 600-nm-thick Ruihong (Suzhou Ruihong Co., China), a positive photoresist, was applied (soft-bake in oven: 65 °C for 5 min; rise to 95 °C with a ramp of 2 °C/min; 95 °C for 5 min) (Figure 1D). The substrate was then aligned and exposed using a photomask with the pattern of metal tracks (UV exposure: g-line, 58 mJ/cm^2; development: 0.4% NaOH, 1 min) (Figure 1E). After the development, ion-beam etching was carried out until the metal uncovered by the photoresist was completely removed (Figure 1F). The remained positive photoresist was removed with ethanol and the substrate was cleaned in oxygen plasma for 1 min (30 W, ME-3A MEIRE, Institute of Microelectronics, China).

Insulating SU-8 Layer Fabrication. A 2-μm-thick SU-8 (SU-8 2002, MicroChem, U.S.) layer was applied as the insulating layer upon the metal tracks (soft-bake in oven: 65 °C for 5 min; rise to 95 °C with a ramp of 2 °C/min; 95 °C for 5 min) (Figure 1G) and patterned using a photomask with the MEA shape, microelectrode holes, and the contact pads (i-line, 28 mJ/cm^2). The PEB was performed in the oven (65 °C for 5 min; rise to 85 °C with a ramp of 2 °C/min; 85 °C for 10 min) (Figure 1H). Then, the substrate was developed in SU-8 Developer (MicroChem Inc., U.S.) for 30 min. MEAs would detach from the glass plate automatically. They were rinsed in isopropyl alcohol immediately after the development. Later, a hard bake was carried out (65 °C for 5 min; rise to 95 °C with a ramp of 2 °C/min; 95 °C for 5 min) to improve the cross-link density of the insulating SU8 layer (Figure 1I).

Packaging. In the final step, copper wires were attached to the contact pads with silver conductive paint (SPI no. 5002, U.S.), and the pads were insulated by silicon rubber (NANDA no. 703, Nanjing Daxue Ltd., China).

A scanning electron microscopy (SEM) image of the microelectrodes on the MEA needle was obtained on a nanoengineering workstation (e-LINE, Raith Co., Germany).

Electrochemical Analysis. An electrochemical detector (CHI 800, CH Instruments Inc., U.S.) was used for electrochemical measurements at 25 °C. Three-electrode configuration was composed of a commercial Ag/AgCl reference electrode (CHI111, CH Instruments Inc., U.S.), a platinum wire counterelectrode (CHI115, CH Instruments Inc., U.S.), and a working gold microelectrode.

Chronoamperometry was used to measure the DO concentration with a cathode polarized potential of −0.75 V (vs Ag/AgCl). The DO level for microelectrode calibration was controlled by saturating the solution with the standard gas containing 0%, 5%, 10%, 15%, or 21% of oxygen, respectively.

DO Measurements for an Aerobic Granule. A column-type sequencing batch reactor (SBR) was used to cultivate aerobic granules as previously described (*21*). When the granules were sampled, the influent synthetic wastewater of the SBR was composed as follows (unit in mg/L): NH_4Cl 391; K_2HPO_4 40; $CaCl_2$ 10; $MgCl_2 \cdot 6H_2O$ 5; $FeSO_4 \cdot 7H_2O$ 4.2. The pH was kept in a range of 7.0−8.5 through dosing $NaHCO_3$ solution. Aerobic granules (Figure 2A) with a diameter of about 3 mm, and fresh effluent from the SBR was sampled for DO measurements. The effluent contained NH_4^+−N of 189 mg/L, NO_2^-−N of 206 mg/L and NO_3^-−N of 31 mg/L.

A flow-cell system, including bubbling, liquid cycle, and measurement devices, was designed for the DO measurement of the granules (Figure 2B). The sampled granule was immediately transferred into the flow cell and carefully settled on the nylon net. The fresh effluent of the SBR was used as

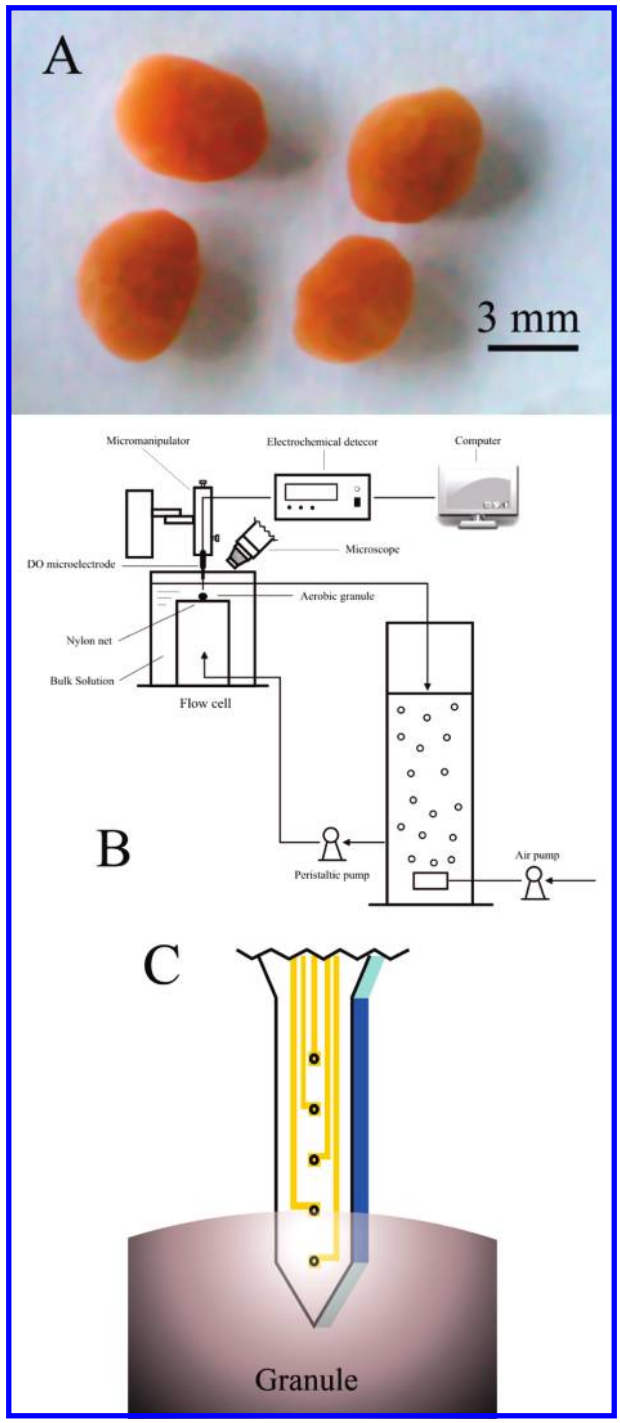

FIGURE 2. (A) Photograph of the aerobic granules; (B) Schematic diagrams of the flow cell system for the DO measurement of the aerobic granules; and (C) MEA needle position during the measurement.

the bulk solution and the fabricated MEA was employed for the DO measurement. Two-point calibrations of the working electrodes were performed before and after the test in the bulk solution with a commercial DO sensor (MO128, Mettler-Toledo Gmbh, Switzerland). The variations of DO response were less than 5%. A micromanipulator was used to adjust the positions of the MEA at a spatial resolution of better than 5 μm, and a microscope was used to precisely locate the granular surface. The needle of the MEA was perpendicularly inserted into the granule, and the second working electrode from the needle tip was positioned at the surface of the granule throughout the test (Figure 2C).

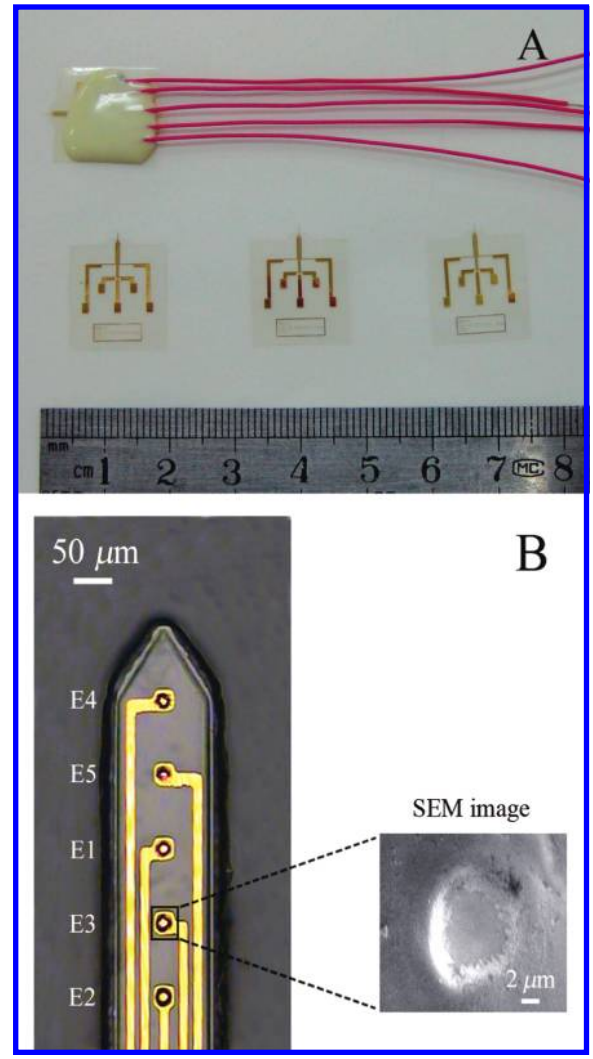

FIGURE 3. (A) Photograph of the fabricated MEAs; (B) Microphotograph and SEM images of the MEA needle (E1−E5: symbols of the working electrodes, the one with biggest response first).

A DO level of the bulk solution was kept stable for 30 min to achieve pseudosteady-state. Then, a DO microprofile near the granular surface was recorded with the five working electrodes on the MEA at five positions. After that, the DO concentration of the bulk solution was changed by adjusting the air and liquid flow rates of the flow cell system. Another 30 min was allowed to reach a new pseudosteady-state before the DO microprofile was recorded again. Totally, three DO microprofiles were measured under three different bulk DO levels. The bulk DO levels of the three tests were 5.32 ± 0.02, 3.80 ± 0.03, and 2.79 ± 0.03 g/m^3, respectively. These figures were measured using the commercial DO sensor mentioned above. No buckling or breaking of the needle was observed during the measurements, and the granule structure had no significant change.

Results and Discussion

Design and Fabrication of the MEA. The MEA contained five gold working electrodes, which located along the axis of a needle (130 μm wide, 92 μm thick, and 1100 μm long) with an interval of 100 μm (Figure 3). The working electrode was design as a 20 $\times$ 20 μm square, but the actual shape of the electrode was typically like a cycle. This was caused by the diffusion of the radicals, which initiated the cross-link of SU8, at the square corners during the expose and PEB

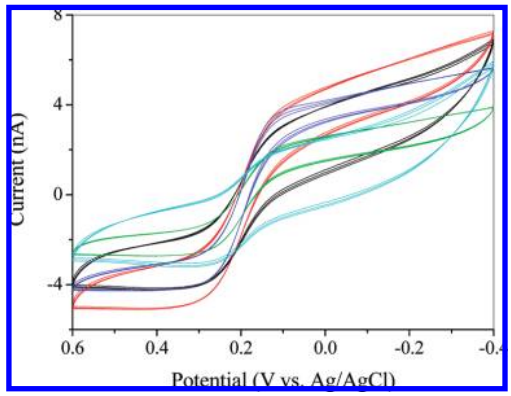

FIGURE 4. Cyclic voltammograms of the five working electrodes on the same MEA in a solution containing 0.005 M ferro/ferricyanide and 0.1 M KCl (scan rate: 0.1 V/s).

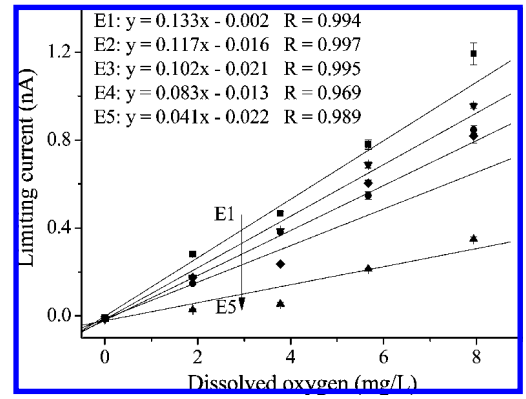

FIGURE 5. DO calibration curves of the five working electrodes on the same MEA in 0.1 M KCl solution.

processes. This diffusion also made the actual area of the working electrode smaller than the designed one. Since a slightly excessive expose dose would result in an exaggerated negative sidewall profile of the electrode holes in the insulating SU-8 layer, the expose dose and PEB of the upper SU8 layer were carefully adjusted, otherwise the microholes would be sealed by the T-topping sidewall.

The MEA could fulfill five-channel analysis at five positions, which was much more powerful than our previous two-channel one-site one. Their schematic diagram could be found in the Supporting Information. It should be noticed that the device shape and microelectrode arrangement were defined by photolithography in this fabrication procedure. Thus, the MEA's shape, microelectrode number, and their positions all could be facilely changed by redesigning the corresponding photo mask(s). Therefore, the procedure proposed in this work provides the control ability both in device shape and electrode arrangement, and is appropriate for the fabrications of various MEAs for multianalysis at different positions.

Evaluation of the MEA in Ferro/Ferricyanide Solution. Cyclic voltammetry analysis of the five working electrodes on one MEA was carried out in a solution containing 0.005 M ferro/ferricyanide and 0.1 M KCl at a scan rate of 0.1 V/s (Figure 4). All cyclic voltammograms showed fine sigmoidal oxidation and reduction waves, which was the typical feature of microelectrode. The peak currents and the shapes of the five voltammograms were similar to each other, showing the coherence of the microelectrodes. The voltammograms were reversible, indicating that the working electrodes were stable and reliable.

Performance of the MEA as a DO Sensor. Chronoamperometry was employed for DO measurement in 0.1 M KCl. The time for 90% response was typically less than 15 s, which was much shorter than those of the usually sized commercial oxygen electrodes.

Calibration curves of the five working electrodes on the same MEA are illustrated in Figure 5. All of the correlation coefficients were greater than 0.96, demonstrating that the microelectrodes had a good linear response to DO. The response ranged from 41 to 133 pA per mg O_2/L, which should be attributed to the differences of the microholes in the insulating SU8 layer formed in the microfabrication. This response range is still acceptable for the simultaneous measurement of usual environmental samples like aerobic granules and comparable to those of other reported MEAs (*19, 20*). The DO response is greater than that of the conventional pulled-pipet ones (typically several pA per mg O_2/L) (*23, 24*), probably attributed to the different electrode areas used.

Lifetimes of the microelectrodes on the same MEA are shown in Figure 6. A 10−15% fluctuation of the DO response

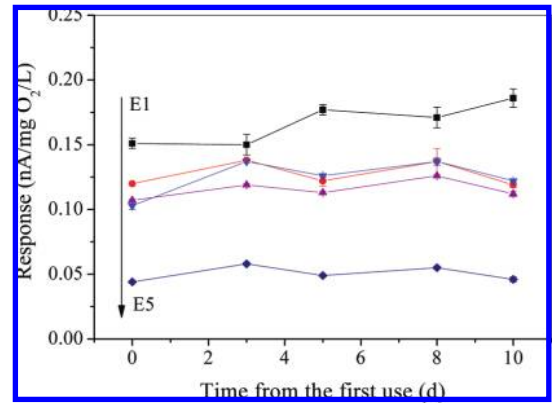

FIGURE 6. Lifetimes of the five working electrodes on the same MEA for DO measurement. The MEA was stored in air.

was observed in 10 days, indicating its good stability. The lifetime of this MEA was much longer than that we previously reported (*21*). This is probably attributed to the high surface energy of the previous microelectrode. In our previous work, the microelectrode surface was revealed by excision, which would cause defects on the gold surface and result in a high surface energy. Surface with a high energy tends to adsorb materials to lower its energy, thus, it is easy to stain and cause an unstable response. In the present work, however, the electrode surface was formed by sputtering deposition. Defects seldom existed on the surface, resulting in more constant electrode characteristics.

Application of the MEA in an Aerobic Granule. Previous studies demonstrated that aerobic granules are delaminated (*21, 30, 31*). Granules have been found to have different structures, microbial communities, and densities at different depths. As a consequence, the parameters in granule models should be different in different layers, rather than be constant thoughout the entire granule.

Typically, the most important layer of an aerobic granule is the most upper layer. It generally has the highest bioactivity, and most diffusional oxygen from bulk liquid was consumed on the upper layer. The granule center was under anaerobic conditions, although the surrounding liquid had a relatively high DO level. In this case, no aerobic oxidation could occur in the inner layer of the aerobic granule because of the oxygen transfer limitation. This observation shown in Figure 7 is consistent with the results of DO distribution in aerobic granules reported previously (*21, 30, 31*). Taking advantage of the special microelectrode arrangement of the MEA fabricated in this work, experiments were designed to measure the oxygen effective diffusivity (D_{eff}) and the DO consumption kinetic parameters in the upper 100 μm layer of an aerobic granule. Three DO microprofiles near the

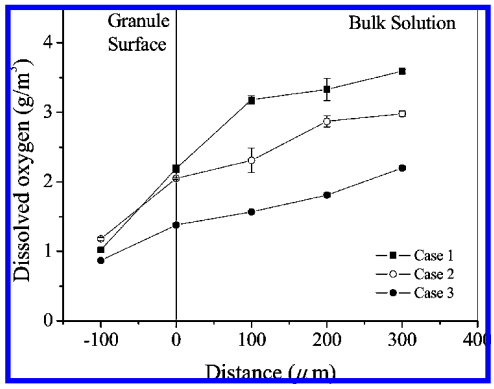

FIGURE 7. DO profiles near the surface of the aerobic granule under the three conditions (bulk DO levels for cases 1, 2, and 3 were 5.32 ± 0.02, 3.80 ± 0.03, and 2.79 ± 0.03 g/m³, respectively).

TABLE 1. Linear Regression Results of Eq 2 and the Calculated $J_{s,w}$ at the Three Bulk DO Levels

case	A (m^{-1})	R^2	$J_{s,w}$ ($g/m^2/s$)	bulk DO concentration (g/m^3)
1	1.96×10^3	0.998	1.54×10^{-5}	5.32 ± 0.02
2	2.66×10^3	0.947	1.16×10^{-5}	3.80 ± 0.03
3	2.46×10^3	0.897	8.67×10^{-6}	2.79 ± 0.03

granular surface were recorded under three different bulk DO levels with the MEA (Figure 7). Values on the x-axis indicate the distance from the granular surface to the monitoring point (in μm) and the positive direction heads the bulk solution. With the MEA, the DO microprofiles near the granule surface under these conditions were obtained without repeated insertion into the granule. This simplified the experimental operations, and more importantly, minimized the destruction of the sample.

A mathematical model was established to estimate the D_{eff} and the kinetic parameters. Since the flow rate in the flow cell was low, the oxygen transport on the stagnant liquid layer above the granule surface should be dominated by diffusion. Therefore, the DO level on the stagnant layer could be described by the following empirical equation:

$$\frac{C - C_0}{C_b - C_0} = 1 - \exp(-AZ) \tag{1}$$

where C is the local DO level, C_0 is the DO concentration at the granule surface, C_b is the DO level in the bulk solution, Z is the distance from the granule surface, and A is an experimental constant, which could be determined by linear regression from the following transform of eq 1:

$$\ln\left(1 - \frac{C - C_0}{C_b - C_0}\right) = -AZ \tag{2}$$

The DO transport flux from the solution into the granule surface ($J_{s,w}$) could be calculated as follows:

$$J_{s,w} = D_w\left(\frac{dC}{dZ}\right)_{w|Z=0} \tag{3}$$

where D_w is the oxygen diffusivity through water, which is 2.5×10^{-9} m^2/s at 25 °C (*32*), subscript s represents granule surface, and subscript w represents water. In the boundary layer

$$\left(\frac{dC}{dZ}\right)_{w|Z=0} = A(C_0 - C_b) \tag{4}$$

Thus, $J_{s,w}$ could be expressed as

$$J_{s,w} = D_w A(C_0 - C_b) \tag{5}$$

The regression results of eq 2 and the calculated $J_{s,w}$ under these conditions are summarized in Table 1.

By taking the diffusion and microbial consumption of oxygen into account, the transport of DO through the granule could be described as shown below:

$$\frac{\partial C}{\partial t} = D_{eff}\left(\frac{\partial^2 C}{\partial Z^2}\right) - \frac{V_{max}C}{K_m + C} \tag{6}$$

where the consumption is expressed by the Monod equation, V_{max} is the maximum oxygen utilization rate, K_m is the half-saturation coefficient, and t is the time.

At steady-state, $\partial C/\partial t = 0$, so

$$D_{eff}\left(\frac{\partial^2 C}{\partial Z^2}\right) = \frac{V_{max}C}{K_m + C} \tag{7}$$

After integrating eq 7 with the following boundary conditions

$$C = C_0, \text{ at } Z = 0$$

$$C = C_{-100}, \text{ at } Z = -100$$

The following equation is obtained:

$$\left(\frac{dC}{dZ}\right)_{g|Z=0} = \sqrt{2\frac{V_{max}}{D_{eff}}\left(C_0 - C_{-100} - K_m \ln\frac{K_m + C_0}{K_m + C_{-100}}\right)} \tag{8}$$

where subscript g represents granule. Consequently, the DO transport flux from the granule surface to the inner part of the granule ($J_{s,g}$) could be calculated as (*33*):

$$J_{s,g} = D_{eff}\left(\frac{dC}{dZ}\right)_{g|Z=0}$$

$$= D_{eff}\sqrt{2\frac{V_{max}}{D_{eff}}\left(C_0 - C_{-100} - K_m \ln\frac{K_m + C_0}{K_m + C_{-100}}\right)} \tag{9}$$

At the granule surface, the DO flux should be a constant under steady-state conditions, i.e., $J_{s,w}$ should equal to $J_{s,g}$. Therefore, a set of D_{eff}, V_{max}, and K_m, could be selected as the appropriate parameters for the tested granule when the $J_{s,g}$ calculated from eq 9 is closest to the measured $J_{s,w}$ under the three investigated DO levels.

A C++ program was written and executed to search for the best set of D_{eff}, V_{max}, and K_m, which minimized the sum of $((J_{s,g} - J_{s,w})/J_{s,w})^2$ under the three conditions, in the reasonable ranges of the parameters (5.0×10^{-10} $m^2/s \le D_{eff} \le 2.5 \times 10^{-9}$ m^2/s; 0.01 $g/m^3/s \le V_{max} \le 10$ $g/m^3/s$; 0.1 $g/m^3 \le K_m \le 3$ g/m^3). The calculation results were $D_{eff} = 1.19 \times 10^{-9}$ m^2/s, $V_{max} = 0.14$ $g/m^3/s$, and $K_m = 1.43$ g/m^3, with the sum of $((J_{s,g} - J_{s,w})/J_{s,w})^2$ equal to 0.00964. This D_{eff} value is comparable to that of an acetate-fed aerobic granule and greater than that of a phenol-fed granule in their upper 125 μm layers (*30*). Jang et al. used a biofilm's D_{eff} value of 1.67×10^{-9} m^2/s in their granule model (*31, 34*), whereas Li and Liu assumed 2.0×10^{-9} m^2/s for that (*35*). Our results suggest that they might slightly overestimate the oxygen diffusion ability in aerobic granules.

Acknowledgments

We thank the Natural Science Foundation of China (20577048, 50625825, and 50738006), and the National Synchrotron Radiation Laboratory for the partial support of this study.

Supporting Information Available

Schematic diagram of the microelectrode needles fabricated in this work and in our previous work.This material is available free of charge via the Internet at http://pubs.acs.org.

Literature Cited

(1) Jang, A.; Lee, J. H.; Bhadri, P. R.; Kumar, S. A.; Timmons, W.; Beyette, F. R.; Papautsky, I.; Bishop, P. L. Miniaturized redox potential probe for in situ environmental monitoring. *Environ. Sci. Technol.* **2005**, *39*, 6191–6197.

(2) Herdan, J.; Feeney, R.; Kounaves, S. P.; Flannery, A. F.; Storment, C. W.; Kovacs, G. T. A.; Darling, R. B. Field evaluation of an electrochemical probe for in situ screening of heavy metals in groundwater. *Environ. Sci. Technol.* **1998**, *32*, 131–136.

(3) Tercier-Waeber, M. L.; Belmont-Hebert, C.; Buffle, J. Real-time continuous Mn(II) monitoring in lakes using a novel voltammetric in situ profiling system. *Environ. Sci. Technol.* **1998**, *32*, 1515–1521.

(4) Gross, P. G.; Kartalov, E. P.; Scherer, A.; Weiner, L. P. Applications of microfluidics for neuronal studies. *J. Neurol. Sci.* **2007**, *252*, 135–143.

(5) Dam, V. A. T.; Olthuis, W.; van den Berg, A. Redox cycling with facing interdigitated array electrodes as a method for selective detection of redox species. *Analyst* **2007**, *132*, 365–370.

(6) Berduque, A.; Lanyon, Y. H.; Beni, V.; Herzog, G.; Watson, Y. E.; Rodgers, K.; Stam, F.; Alderman, J.; Arrigan, D. W. M. Voltammetric characterisation of silicon-based microelectrode arrays and their application to mercury-free stripping voltammetry of copper ions. *Talanta* **2007**, *71*, 1022–1030.

(7) Hochberg, L. R.; Serruya, M. D.; Friehs, G. M.; Mukand, J. A.; Saleh, M.; Caplan, A. H.; Branner, A.; Chen, D.; Penn, R. D.; Donoghue, J. P. Neuronal ensemble control of prosthetic devices by a human with tetraplegia. *Nature* **2006**, *442*, 164–171.

(8) Stett, A.; Egert, U.; Guenther, E.; Hofmann, F.; Meyer, T.; Nisch, W.; Haemmerle, H. Biological application of microelectrode arrays in drug discovery and basic research. *Anal. Bioanal. Chem.* **2003**, *377*, 486–495.

(9) Lee, J.-H.; Jang, A.; Bhadri, P. R.; Myers, R. R.; Timmons, W., Jr.; Bishop, P. L.; Papautsky, I. Fabrication of microelectrode arrays for in situ sensing of oxidation reduction potentials. *Sens. Actuator, B* **2006**, *115*, 220–226.

(10) Gobet, J.; Rychen, P.; Cardot, F.; Santoli, E. Microelectrode array sensor for water quality monitoring. *Water Sci. Technol.* **2003**, *47*, 127–134.

(11) Tomcik, P.; Jencusova, P.; Krajcikova, M.; Bustin, D.; Brescher, R. The detection of formaldehyde in textiles using interdigitated microelectrode array diffusion layer titration with electrogenerated hypobromite. *Anal. Bioanal. Chem.* **2005**, *383*, 864–868.

(12) Wilson, M. S.; Nie, W. Y. Electrochemical multianalyte immunoassays using an array-based sensor. *Anal. Chem.* **2006**, *78*, 2507–2513.

(13) Lowinsohn, D.; Peres, H. E. M.; Kosminsky, L.; Paixao, T. R. L. C.; Ferreira, T. L.; Ramirez-Fernandez, F. J.; Bertotti, M. Design and fabrication of a microelectrode array for iodate quantification in small sample volumes. *Sens. Actuator, B* **2006**, *113*, 80–87.

(14) Errachid, A.; Ivorra, A.; Aguilo, J.; Villa, R.; Zine, N.; Bausells, J. New technology for multi-sensor silicon needles for biomedical applications. *Sens. Actuator, B* **2001**, *78*, 279–284.

(15) Rajaraman, S.; Choi, S.-O.; Shafer, R. H.; Ross, J. D.; Vukasinovic, J.; Choi, Y.; DeWeerth, S. P.; Glezer, A.; Allen, M. G. Microfabrication technologies for a coupled three-dimensional microelectrode, microfluidic array. *J. Micromech. Microeng.* **2007**, *17*, 163–171.

(16) Jung, D. R.; Kapur, R.; Adams, T.; Giuliano, K. A.; Mrksich, M.; Craighead, H. G.; Taylor, D. L. Topographical and physicochemical modification of material surface to enable patterning of living cells. *Crit. Rev. Biotechnol.* **2001**, *21*, 111–154.

(17) Najafi, K.; Wise, K. D.; Mochizuki, T. High-Yield IC-Compatible Multichannel Recording Array. *IEEE Trans. Electron Devices* **1985**, *32*, 1206–1211.

(18) Lin, L.; Pisano, A. P. Silicon-processed microneedles. *J. Microelectromech. Syst.* **1999**, *8*, 78–84.

(19) Lee, J. H.; Seo, Y.; Lim, T. S.; Bishop, P. L.; Papautsky, I. MEMS needle-type sensor array for in situ measurements of dissolved oxygen and redox potential. *Environ. Sci. Technol.* **2007**, *41*, 7857–7863.

(20) Lee, J. H.; Lim, T. S.; Seo, Y.; Bishop, P. L.; Papautsky, I. Needle-type dissolved oxygen microelectrode array sensors for in situ measurements. *Sens. Actuator, B* **2007**, *128*, 179–185.

(21) Liu, S.-Y.; Liu, G.; Tian, Y.-C.; Chen, Y.-P.; Yu, H.-Q.; Fang, F. An innovative microelectrode fabricated using photolithography for measuring dissolved oxygen distributions in aerobic granules. *Environ. Sci. Technol.* **2007**, *41*, 5447–5452.

(22) Liu, S.-Y.; Chen, Y.-P.; Fang, F.; Li, S.-H.; Ni, B.-J.; Liu, G.; Tian, Y.-C.; Xiong, Y.; Yu, H.-Q. An innovative solid-state microelectrode for nitrite determination in a nitrifying granule. *Environ. Sci. Technol.* **2008**, *42*, 4467–4471.

(23) Linsenmeier, R. A.; Yancey, C. M. Improved fabrication of double-barreled recessed cathode O_2 microelectrodes. *J. Appl. Physiol.* **1987**, *63*, 2554–2557.

(24) Bezbaruah, A. N.; Zhang, T. C. An innovative electro-corrosion recess creation technique for improved microelectrode fabrication. *Water Res.* **2002**, *36*, 4428–4432.

(25) McRipley, M. A.; Linsenmeier, R. A. Fabrication of a mediated glucose oxidase recessed microelectrode for the amperometric determination of glucose. *J. Electroanal. Chem.* **1996**, *414*, 235–246.

(26) Goral, V. N.; Zaytseva, N. V.; Baeumner, A. J. Electrochemical microfluidic biosensor for the detection of nucleic acid sequences. *Lab Chip* **2006**, *6*, 414–421.

(27) Liu, Y.; Tay, J. H. State of the art of biogranulation technology for wastewater treatment. *Biotechnol. Adv.* **2004**, *22*, 533–563.

(28) Su, K.-Z.; Yu, H.-Q. A generalized model for aerobic granule-based sequencing batch reactor. 1. Model development. *Environ. Sci. Technol.* **2006**, *40*, 4703–4708.

(29) Su, K.-Z.; Yu, H.-Q. A generalized model for aerobic granule-based sequencing batch reactor. 2. Parametric sensitivity and model verification. *Environ. Sci. Technol.* **2006**, *40*, 4709–4713.

(30) Chiu, Z. C.; Chen, M. Y.; Lee, D. J.; Wang, C. H.; Lai, J. Y. Oxygen diffusion in active layer of aerobic granule with step change in surrounding oxygen levels. *Water Res.* **2007**, *41*, 884–892.

(31) Jang, A.; Yoon, Y.-H.; Kim, I. S.; Kim, K.-S.; Bishop, P. L. Characterization and evaluation of aerobic granules in sequencing batch reactor. *J. Biotechnol.* **2003**, *105*, 71–82.

(32) *Perry's Chemical Engineers' Handbook*, 6th ed.; Perry, R. H.; Green, D. W., Eds.; McGraw-Hill Inc.: New York, 1984.

(33) Lewandowski, Z.; Walser, G.; Characklis, G. Reaction kinetics in biofilms. *Biotechnol. Bioeng.* **1991**, *38*, 877–882.

(34) Chen, S.; Juaw, C.; Cheng, S. Nitrification and denitrification of high-strength ammonium and nitrite wastewater with biofilm reactors. *Water Sci. Technol.* **1991**, *23*, 1417–1425.

(35) Li, Y.; Liu, Y. Diffusion of substrate and oxygen in aerobic granule. *Biochem. Eng. J.* **2005**, *27*, 45−52.

ES802662E